Photoacoustic tomography of carrageenan-induced arthritis in a rat model

David L. Chamberland*
University of Michigan School of Medicine
Division of Rheumatology
Department of Internal Medicine
Ann Arbor, Michigan 48109

Xueding Wang
University of Michigan School of Medicine
Department of Radiology
Ann Arbor, Michigan 48109

Blake J. Roessler
University of Michigan School of Medicine
Division of Rheumatology
Department of Internal Medicine
Ann Arbor, Michigan 48109

Abstract. Laser-based photoacoustic tomography (PAT), a novel, nonionizing, noninvasive, laser-based technology, has been adapted to the diagnosis and imaging of inflammatory arthritis. A commonly used adjuvant induced arthritis model using carrageenan was employed to simulate acute rheumatoid arthritis in rat tail joints. Cross-sectional photoacoustic images of joints affected by acute inflammation were compared to those of the control. The diameter of the periosteum and the optical absorption of intra-articular tissue were measured on each joint image. Significant differences were found on PAT imaging between the affected joints and the control for both variables measured, including enlarged periosteum diameter and enhanced intra-articular optical absorption occurring in the joints affected with carrageenan-induced arthritis. Anatomical correlation with histological sections of imaged joints and microMRI results verified the findings of PAT. This suggests that PAT has the potential for highly sensitive diagnosis and evaluation of pathologic hallmarks of acute inflammatory arthritis.
 [DOI: 10.1117/1.2841028]

Keywords: photoacoustic tomography (PAT); imaging; diagnosis; inflammatory arthritis; joint.

Paper 07085SSRR received Mar. 2, 2007; revised manuscript received Sep. 25, 2007; accepted for publication Oct. 9, 2007; published online Feb. 25, 2008.

1 Introduction

Rheumatoid arthritis (RA), the most common human type of inflammatory arthritis, has a prevalence of approximately 1% in North America.[1] In many cases, RA involves not only joint disease but morbidity involving multiple organs. Erosive RA has been correlated with significant disability[2] and loss of productivity.[3] Given the extent of morbidity involved in RA and the relatively large percentage of the population affected, improvements in diagnostic and therapeutic tools can have a significant impact with this disease. Medical imaging is one area used extensively by primary care physicians and rheumatologists both for diagnostic and therapeutic assessments.

Medical imaging must be optimized for pathologic hallmarks of specific disease entities. Characteristic changes of inflammatory arthritis, such as RA, include aberrant synovial growth and production of inflammatory chemokines capable of destroying adjacent articular cartilage and bone.[4] A critical early event in this pathologic state is neoangiogenesis, the formation of new vessels from existing blood vessels.[5–7] Morphometric studies have also shown that capillary density appears to be increased in the RA synovium.[8] Ironically, in the setting of aberrant synovial proliferation and increased angiogenesis, there is thought to be local relative hypoperfusion and hypoxia.[8,9] Also peri-articular inflammation can increase synovial fluid, thus elevating intra-articular pressure, causing further hypoperfusion of vasculature.[10]

Currently, conventional x-ray is the most commonly used imaging modality for assessment of inflammatory arthritis, including RA, both initially and in follow-up for therapeutic assessment. X-ray is limited, however, in identification of pathologic soft tissue changes. Magnetic resonance imaging (MRI) with gadolinium can provide excellent resolution of soft tissues and bone erosions, but it is very expensive and less accessible and not all patients are able to tolerate the procedure due to having metal implants or claustrophobia. Ultrasound is being used more extensively, as it is better than conventional x-ray in imaging soft tissues, relatively cheap, accessible, and nonionizing. However, with limited sensitivity to tissue inflammation, ultrasound alone cannot be used as a primary screening tool for RA.

Photoacoustic tomography (PAT) is a relatively new laser-based technology that involves application of short-pulsed light to targeted tissues, producing thermoelastic expansion and thus ultrasound waves.[11–16] These mechanical waves are detected, and using a reconstruction algorithm, images are produced. Advantages of PAT include much improved spatial resolution over traditional diffuse optical tomography (DOT). Optical signals are sensitive to molecular conformation of biological tissues, allowing measurement of physiologic parameters such as hemoglobin oxygenation and hemoglobin concentration. PAT has recently been demonstrated successfully for small animal brain structural and functional imaging and is thought to be potentially an optimal imaging modality

*Current address: 1365 Poplar Drive, Medford, OR 97504. E-mail: davicham@med.umich.edu
Address all correspondence to Xueding Wang, Ph.D., University of Michigan, Department of Radiology, Ann Arbor, MI 48109-0553. E-mail: xdwang@umich.edu

1083-3668/2008/13(1)/011005/6/$25.00 © 2008 SPIE

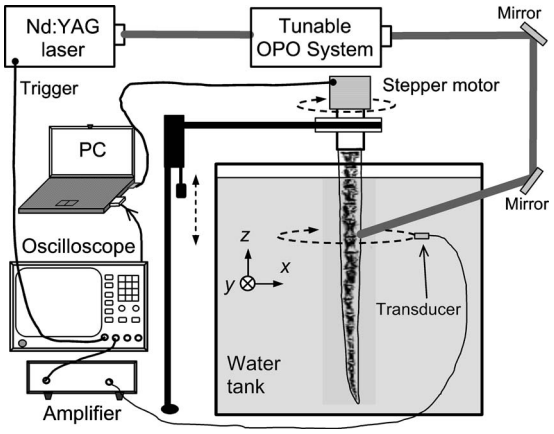

Fig. 1 Schematic of the PAT system for joint imaging.

for inflammatory arthritis, as it is able to characterize soft tissue changes and functional parameters, including tissue oxygen saturation and blood volume, all of which are pathologic characteristics of entities such as RA.[17–22]

Animal models mimicking acute inflammatory arthritis have been used extensively for research purposes. Carrageenan-induced arthritis is a commonly used model in multiple different animal types including rat, dog, and rabbit. It has been validated to produce pathological joint findings, which are thought to be somewhat similar to RA.[23] In this study, PAT was applied successfully for the first time to an animal inflammatory arthritis model. For initial testing of PAT, experiments were designed to detect joint changes involved in acute inflammatory arthritis—namely, periosteum size, which if enlarged in non-weight-bearing situations, can be indicative of swelling—and enhanced intra-articular tissue optical absorption suggesting vascular dilatation and increased blood volume, as hemoglobin, at the wavelength tested, is the dominant absorbing chromophore.

2 Methods

2.1 *Instrumentation Setup*

The PAT system for imaging rat tail joints involves laser pulse generation and delivery, photoacoustic signal reception, and image reconstruction and display, as shown in Fig. 1, where an *x*-*y*-*z* coordinate system is indicated. An OPO system (Vibrant B, Opotek) pumped by an Nd:YAG laser (Brilliant B, Bigsky) is used to provide laser pulses with a pulse repetition rate of 10 Hz and a pulse width of 5.5 ns. In this study, the wavelength of the laser light is tuned by the OPO system to 700 nm, which is in the near-infrared (NIR) region and can enable good penetration in biological tissues. The laser beam irradiates the imaged joint with an input energy density of 15 mJ/cm^2, well below the human ANSI safety limit of 20 mJ/cm^2. The laser light penetrates into the joint tissues and generates photoacoustic signals that are scanned by a small, wideband ultrasonic transducer (XMS-310, Panametrics) around the joint. This transducer has a central frequency of 10 MHz, a bandwidth of 100% at −6 dB, and an element size of 2 mm diameter. To couple the photoacoustic signals, both the sample and the transducer are immersed in a tank of water. After a preamplifier (PR5072, Panametrics), the detected signals are digitized by an oscilloscope (TDS 540B, Tektronics) and then collected by a computer for image reconstruction. To take a two-dimensional (2-D) cross-sectional image through the center of a rat tail joint, the tail was stepped through axial rotation while keeping the transducer and the laser beam static. The scanning time for 2-D imaging of a specimen is 20 min. By using the circular scanning geometry, although the in-plane resolution is good, the vertical resolution is limited and is primarily dependent on the transducer's *z* dimension and the radius of the scanning circle. In order to achieve good spatial resolution along the vertical direction, three-dimensional (3-D) imaging of the joint can be conducted in the future. The details of this imaging system can be found in Ref. 24.

2.2 *Ultrasound Compounding Imaging*

To explore the differences in joint imaging based on tissue optical contrast and mechanical contrast, respectively, the photoacoustic image was compared with an ultrasound compounding image taken along the similar cross section in a joint. The ultrasound images were taken using the GE LOGIQ 9 ultrasound platform with a 10-L linear probe working at 10 MHz. A cross-sectional image of a joint can be acquired by facing the probe toward the joint while the linear probe is perpendicular to the orientation of the joint (i.e., the distribution of the transducer elements is in the *x*-*y* plane and perpendicular to the *z*-axis in Fig. 1). In total, 40 ultrasound images of a joint were taken at 40 positions evenly distributed around the joint, with a constant step of 9 deg to cover the 2π viewing angle. Then a spatial ultrasound compounding image of the cross section was formed after compounding these 40 images incoherently.[25] Compound imaging was employed because it may lead to improved image quality compared with conventional ultrasound, partly because of reduction of speckle and other acoustic artifacts as well as improved contrast resolution and tissue differentiation. Most importantly, conventional ultrasound cannot "see" through the bone, while compound imaging is able to present complete articular tissue structures in a cross section.

2.3 *MicroMRI*

To anatomically correlate PAT results with a known imaging standard, MRI of normal and inflamed rat joints was also conducted. MRI has been involved more and more in early detection and staging of RA due to its good soft tissue contrast and high spatial resolution.[26,27] T_2-weighted MRI images were taken with a 9.4 tesla microMRI system (Inova) at the University of Michigan Center for Molecular Imaging. The spatial resolution in the imaged cross sections was 78 μm, and the slide thickness was 250 μm. For comparison with PAT results, 2-D cross-sectional MRI images, which were also through the center of the imaged joints, are presented. Unlike PAT, which is sensitive to hemoglobin concentration, MRI is more sensitive to the water content in various articular tissues.

2.4 *Animal Samples*

Five pairs of adult Sprague Dawley rats (~300 g, Charles River Laboratory) were included in the study. In each pair, the tail of one rat was induced with inflammatory arthritis, while

the tail of the other rat was kept normal to be used as a control. The two rats in each pair were from the same group, and hence their body weights were very similar. The imaged joint segment in each tail was 2.5 cm distal to the rat trunk; therefore, the initial sizes of the two imaged joints in each pair were also similar. To induce inflammation in the tail joint to be imaged, 0.15 mL of 3% carrageenan (Sigma-Aldrich Co.) solution in physiologic saline was injected intra-articularly. For comparison, we also performed injection of 0.15 mL physiologic saline to the control joint. At 7 to 10 days after injection, when the joint receiving carrageenan had shown clinical signs of inflammation (e.g., swelling and erythema), both the normal and inflamed rat tail joints in each pair were studied in the same day.

Whole tails were harvested from the rat bodies within 1 min after the rats were sacrificed. An electrocautery device (SurgiStat, Valleylab) was then used to clot blood and seal vessels at the proximal cut end of the tail. Before image acquisition, tail hair was removed using hair removal lotion, as it can cause light scattering. Each rat tail was placed in the PAT system along the z axis (see Fig. 1). The first proximal segment of the rat tail was fixed on a rotational stage that, driven by a stepper motor, can rotate the tail around its axis. Normal rat tails were imaged to verify the feasibility of PAT in describing joint tissue structures based on the intrinsic optical contrast. In order to examine the ability of this technology in imaging inflamed joints, images of normal rat tail joints and those affected by carrageenan-induced inflammatory arthritis were compared. 2-D PAT of each joint was performed through a single circular scan around the cross section, which was through the center of the imaged joint.

After all images were recorded, the rat tails were saved in 10% buffered formalin for 3 days. The tails were then decalcified with formic acid for 4 to 7 days and monitored with a Faxitron MX-20 x-ray machine. Once specimen decalcification was completed, they were dehydrated with graded alcohol (Hypercenter XP, Shandon), embedded in paraffin (Paraplast Plus), cut into blocks, and sectioned to 7-μm thickness with a Reichert-Jung 20/30 metal knife (paraffin microtome). Hematoxylin and eosin staining of specimen sections on glass slides was conducted. Last, histological pictures of specimen sections were taken with a 10× magnification.

3 Results

3.1 *PAT and Ultrasound Compounding Imaging*

In the 2-D photoacoustic image of a normal rat tail joint acquired through a circular scan around the cross section [Fig. 2(a)], joint tissue structures are presented successfully based on the intrinsic optical contrast among various soft tissues. With the applied wavelength, the dominant absorption chromophore in articular tissues is hemoglobin; therefore, the contrast of PAT images reveals the spatially distributed concentrations of hemoglobin. The spatial resolution achieved by the current PAT system is about 200 μm which is much better than that achieved by traditional optical imaging of joints.[28–30] Through the comparison with the histological photograph taken along a similar cross section in a rat tail joint [see Fig. 2(c)], some articular tissues, including skin, vessels, and periosteum, are described clearly in the 2-D PAT image. In comparison with the ultrasound compounding image in Fig. 2(b), which is based on the mechanical contrast among articular tissues, photoacoustic results presenting tissue optical contrast reveal more soft tissue features, especially blood vessels and highly vascularized tissues such as periosteum.

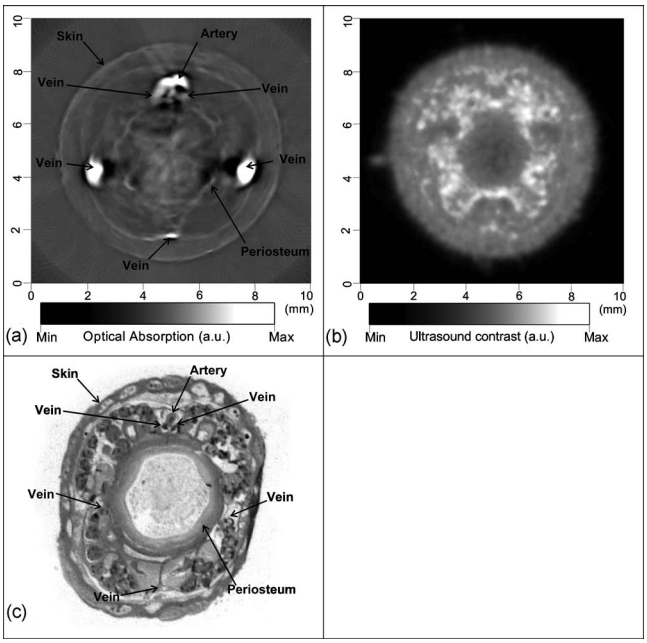

Fig. 2 (A) 2-D photoacoustic image of a cross section in a rat tail joint. (b) Ultrasound compounding image of a similar cross section in the rat tail joint. (c) Histological photograph of a cross section in the rat tail joint taken along the planes as closely matched as possible to those of the PAT and ultrasound images.

3.2 *Imaging of Arthritic Joints*

The 2-D cross-sectional photoacoustic images of rat tail joints affected by inflammatory arthritis were compared to those of the normal samples. Due to the high sensitivity of the optical signal to morphological and physiological tissue properties, PAT shows promise in identifying the changes associated with joint inflammation. Figure 3 shows a pair of imaging results as an example, where Figs. 3(a) and 3(b) correspond to the normal and the affected joints, respectively. First, the periosteum in the inflamed joint is enlarged compared to that of the normal joint. With comparatively strong optical absorption, the periosteum is a white line surrounding the intra-articular tissue in each photoacoustic image. The periosteum in Fig. 3(b) is not presented as clearly as those in Figs. 2(a) and 3(a), which is mainly due to the soft tissue deformation and the enhancement of optical absorption in the inflamed joint. The diameter of the periosteum along the horizontal direction of the joint was measured. The ratio of periosteum diameter between this pair of normal and affected joint samples is about 1:1.09. The expansion of the periosteum in the affected joint is believed to be caused by the swelling due to carrageenan-induced inflammation. Periosteum enlargement was confirmed by the microMRI results shown in Figs. 3(c) and 3(d).

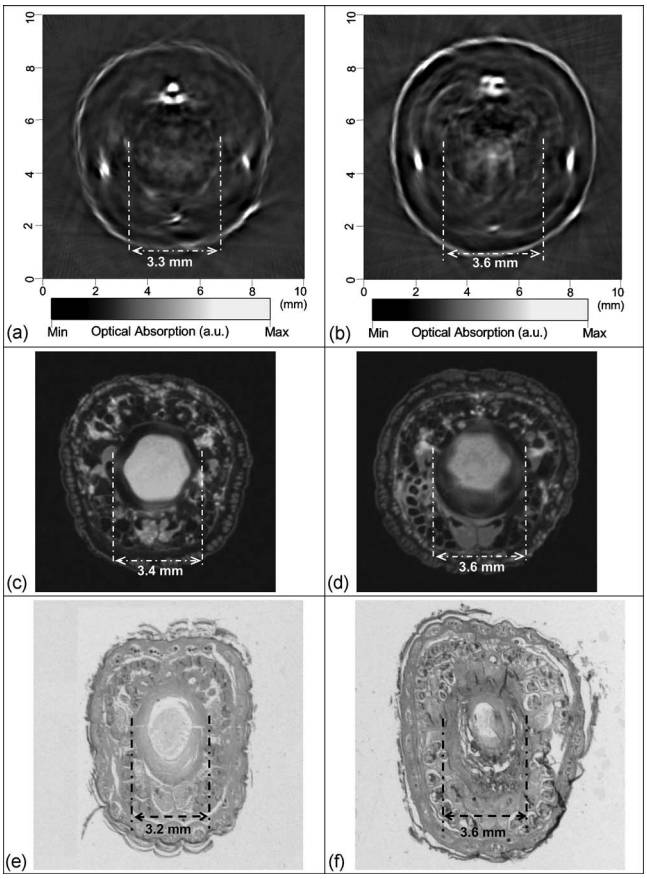

Fig. 3 2-D PAT of the similar cross sections in (a) a normal rat tail joint and (b) a rat tail joint affected by inflammatory arthritis. 2-D microMRI of the similar cross sections in (c) the normal rat tail joint and (d) the rat tail joint affected by inflammatory arthritis. Histological photographs of the cross sections in (e) the normal rat tail joint and (f) the joint affected by inflammatory arthritis taken along the planes as closely matched as possible to those of the PAT and microMRI images.

PAT and MRI findings have also been verified by histological examinations shown in Figs. 3(e) and 3(f), where we can see clearly the expansion of periosteum in the affected joint. MRI and PAT present different tissue contrast, which is at least partially the reason for the small discrepancy between the MRI and the PAT measurements. The small difference between the MRI and the PAT outcomes, as well as the difference between the PAT and the histology findings, may also come from the deformation of soft articular tissues during the image acquisition and the histological examination. In this study, marking the periosteum diameter was realized simply by reading the images or photographs, which may also involve some small errors in the measurements.

Second, the intra-articular tissues in the inflamed joint show higher optical absorption in comparison with those in the normal joint. To prevent potential bias caused by the difference in laser light intensities, the spatially distributed optical absorption presented in each photoacoustic image was normalized to the maximal optical absorption in the areas of venous vessels. The optical absorption from the skin was not used in normalization, because this measurement can be

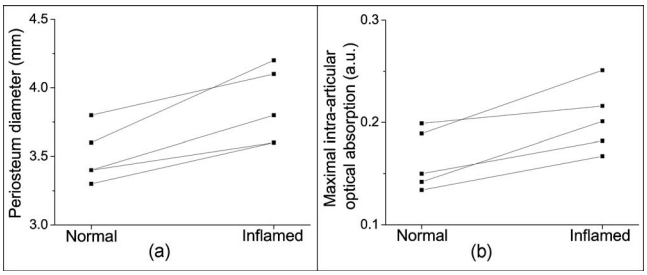

Fig. 4 Measurements of (a) periosteum size and (b) maximal intra-articular optical absorption for five pairs of normal and inflamed rat tail joints.

affected significantly by several parameters, including the skin color, possible stains on the skin surface, and the time period after the tail specimen was immersed in the water. After normalization, the maximal optical absorption in the periosteum and associated intra-articular tissues in each photoacoustic image was measured. For the results in Figs. 3(a) and 3(b), the maximal intra-articular optical absorption of the normal and the affected joints has a ratio of about 1:1.09.

Scattered plots presenting the periosteum diameters and the maximal intra-articular optical absorption for the five pairs of rat tail specimens are shown in Figs. 4(a) and 4(b), respectively. The ratios of the periosteum diameters between the affected joint and the normal joint in each pair for the five pairs of specimens range from 1.09:1 to 1.18:1, with an average number of 1.12 and a standard deviation of 0.05; while the ratios of the maximal intra-articular optical absorption for the five pairs of specimens range from 1.09:1 to 1.41:1, with an average number of 1.26 and a standard deviation of 0.12. Further statistical analysis was also completed to determine whether there were significant differences in periosteum size and maximal intra-articular optical absorption between the measurements from the normal and arthritic joints. A Wilcoxon signed-rank test was conducted because it is the appropriate nonparametric test for comparing the equality of matched pairs of observations. The null hypothesis was that no difference existed between the PAT measurements from the affected joints and the normal joints. There was a statistical difference with regard to each variable ($p < 0.05$).

4 Discussion

As molecular biology continues to decipher new cells, mediators, and pathways implicated in inflammatory arthritis, the radiology and medical instrumentation community continues to develop modalities for further evaluation of inflammatory arthritis for use in both human and animal models. For the first time, PAT has been used in a well-known acute inflammatory arthritis animal model, illustrating its ability to capture important pathologic hallmarks of inflammatory arthritis. While the imaging quality needs improvement, this preliminary study indicates the feasibility of PAT as an important potential modality for evaluation of inflammatory arthritis.

This study documents a significant difference in size of targeted rat tail joint segments post carrageenan injection. In light of the 7 to 10 days allotted in our experiments, joint

pathology more closely mimics acute inflammatory arthritis. Therefore, the enlargement of periosteum observed in this study shows primarily the swelling of itself and associated intra-articular tissue as a result of acute inflammation instead of the joint tissue proliferation, as in chronic inflammatory arthritis. However, for both acute and chronic inflammatory arthritis, morphological changes in periosteum and the associated intra-articular tissues manifest the extent of inflammation during the progression of arthritis. This study suggests the ability of PAT to present the morphology of articular tissues with both optical contrast and high spatial resolution. The quantification of intra-articular tissue swelling by PAT, a potential morphological hallmark of synovitis, would be clinically useful for the diagnosis and therapy of inflammatory arthritis.

Increased optical absorption has also been found in intra-articular tissue of the inflamed joints in comparison with the normal group. As a consequence of the carrageenan-induced inflammatory response, local cytokine production is upregulated, causing vascular dilatation, local endothelial activation, and recruitment of inflammatory cells. PAT is sensitive to dominating chromophores, particularly hemoglobin, and the enhanced local blood flow and thus hemoglobin content in intra-articular tissue may be primarily responsible for the increased optical absorption. Given the acute arthritis model, it is likely that significant increased angiogenesis has not yet occurred. The hemodynamic change, or to be specific, enhanced blood volume, in regional arthritic tissues is another potential hallmark of synovitis. Imaging and quantifying this hallmark of synovitis potentially enables objective assessment of the progression and degree of inflammatory arthritic diseases.

Noticeable artifacts can be recognized in the current PAT images of joints, which, for example, likely cause the periosteum and skin to not be consistently presented. Image artifacts are at least in part a consequence of the acoustic heterogeneity of joint tissues. For example, the speed of sound used in image reconstruction was 1.5 mm/μs in this study. The small variation of speed of sound in articular tissues may cause distortion of photoacoustic wave propagation and induce focus errors in synthetic aperture image reconstruction. Moreover, the reflection of photoacoustic signals from bone surface as well as the inhomogeneous distribution of light fluence in the imaged cross section can be other potential sources of artifact. Part of our future research will be focused on understanding and minimizing these problems.

Acknowledgments

The authors thank Drs. Paul L. Carson, J. Brian Fowlkes, and Jingping Xu at the University of Michigan and Dr. Lihong V. Wang at Washington University for useful discussions and suggestions. The authors also thank Emily Somers for her help in statistical analysis. This work was supported in part by the Arthritis National Research Foundation.

References

1. J. J. Goronzy, C. M. Weyand, R. J. Anderson, E. L. Matteson, "Rheumatoid arthritis," in *Primer on the Rheumatic Diseases*, 12th ed., J. H. Klippel Ed., pp. 209–232, Arthritis Foundation, Atlanta (2001).
2. K. W. Drossaers-Bakker, M. de Buck, D. van Zeben, A. H. Zwinderman, F. C. Breedveld, and J. M. Hazes, "Long-term course and outcome of functional capacity in rheumatoid arthritis: the effect of disease activity and radiologic damage over time," *Arthritis Rheum.* **42**, 1854–1860 (1999).
3. K. Puolakka, H. Kautiainen, M. Pekurinen, T. Mottonen, P. Hannonen, M. Korpela, M. Hakala, M. Arkela-Kautianinen, R. Luukkainen, and M. Leirisalo-Repo, "Monetary value of lost productivity over a 5-year follow up in early rheumatoid arthritis estimated on the basis of official register data on patients' sickness absence and gross income: experience from the FIN-RACo trial," *Ann. Rheum. Dis.* **65**, 899–904 (2005).
4. R. H. Mullan, B. Bresnihan, L. Golden-Mason, T. Markham, R. O'Hara, O. FitzGerald, D. J. Veale, and U. Fearon, "Acute-phase serum amyloid: a stimulation of angiogenesis, leukocyte recruitment, and matrix degradation in rheumatoid arthritis through an NF-kappaB-dependent signal transduction pathway," *Arthritis Rheum.* **54**, 105–114 (2006).
5. U. Fearon, K. Griosios, A. Fraser, R. Reece, P. Emery, P. F. Jones, and D. J. Veale, "Angiopoietins, growth factors, and vascular morphology in early arthritis," *J. Rheumatol.* **30**, 260–268 (2003).
6. R. J. Reece, J. D. Canete, W. J. Parsons, P. Emery, and D. J. Veale, "Distinct vascular patterns of early synovitis in psoriatic, reactive, and rheumatoid arthritis," *Arthritis Rheum.* **42**, 1481–1484 (1999).
7. A. E. Koch, "Angiogenesis as a target in rheumatoid arthritis," *Ann. Rheum. Dis.* **62**(Suppl. 2), 60–67 (2003).
8. O. FitzGerald, M. Soden, G. Yanni, R. Robinson, and B. Bresnihan, "Morphometric analysis of blood vessels in synovial membranes obtained from clinically affected and unaffected knee joints of patients with rheumatoid arthritis," *Ann. Rheum. Dis.* **50**, 792–796 (1991).
9. E. M. Paleolog, "Angiogenesis in rheumatoid arthritis," *Arthritis Care Res.* **4**(Suppl. 3), S81–90 (2002).
10. A. I. Richman, E. Y. Su, and G. Ho, "Reciprocal relationship of synovial fluid volume and oxygen tension," *Arthritis Rheum.* **24**, 701–705 (1981).
11. C. G. A. Hoelen, F. F. M. de Mul, R. Pongers, and A. Dekker, "Three-dimensional photoacoustic imaging of blood vessels in tissue," *Opt. Lett.* **23**, 648–650 (1998).
12. R. O. Esenaliev, A. A. Karabutov, and A. A. Oraevsky, "Sensitivity of laser opto-acoustic imaging in detection of small deeply embedded tumors," *IEEE J. Sel. Top. Quantum Electron.* **5**, 981–988 (1999).
13. R. O. Esenaliev, I. V. Larina, K. V. Larin, D. J. Deyo, M. Motamedi, and D. S. Prough, "Optoacoustic technique for noninvasive monitoring of blood oxygenation: a feasibility study," *Appl. Opt.* **41**, 4722–4731 (2002).
14. R. A. Kruger, D. R. Reinecke, and G. A. Kruger, "Thermoacoustic computed tomography—technical considerations," *Med. Phys.* **26**, 1832–1837 (2003).
15. M. Xu and L. V. Wang, "Photoacoustic imaging in biomedicine," *Rev. Sci. Instrum.* **77**, 041101 (2006).
16. H. F. Zhang, K. Maslov, G. Stoica, and L. V Wang, "Functional photoacoustic microscopy for high-resolution and noninvasive *in vivo* imaging," *Nat. Biotechnol.* **24**, 848–851 (2006).
17. X. Wang, Y. Xu, M. Xu, S. Yokoo, E. S. Fry, and L.-H. Wang, "Photoacoustic tomography of biological tissues with high cross-section resolution: reconstruction and experiment," *Med. Phys.* **29**, 2799–2805 (2002).
18. X. Wang, G. Ku, M. A. Wegiel, D. J. Bornhop, G. Stoica, and L. V. Wang, "Noninvasive photoacoustic angiography of animal brains *in vivo* with near-infrared light and an optical contrast agent," *Opt. Lett.* **29**, 730–732 (2004).
19. X. Wang, Y. Pang, G. Ku, X. Xie, G. Stoica, and L. V. Wang, "Noninvasive laser-induced photoacoustic tomography for structural and functional imaging of the brain *in vivo*," *Nat. Biotechnol.* **21**, 803–806 (2003).
20. X. Wang, D. L. Chamberland, , and D. A. Jamadar, "Noninvasive photoacoustic tomography of human peripheral joints toward diagnosis of inflammatory arthritis," *Opt. Lett.* **32**, 3002–3004 (2007).
21. X. Wang, X. Xie, G. Ku, G. Stoica, and L. V. Wang, "Noninvasive imaging of hemoglobin concentration and oxygenation in the rat brain using high-resolution photoacoustic tomography," *J. Biomed. Opt.* **11**, 024015 (2006).
22. X. Wang, G. Ku, X. Xie, Y. Wang, G. Stoica, and L. V. Wang, "Noninvasive functional photoacoustic tomography of blood-oxygen saturation in the brain," *Proc. SPIE* **5320**, 69–76 (2004).

23. P. Hansra, E. Moran, V. Fornasier, and E. Boguch, "Carrageenan-induced arthritis in the rat," *Inflammation* **24**, 141–155 (2000).
24. X. Wang, D. L. Chamberland, P. L. Carson, J. B. Fowlkes, R. O. Bude, and D. A. Jamadar, "Imaging of joints with laser-based photoacoustic tomography: an animal study," *Med. Phys.* **33**, 2691–2697 (2006).
25. P. R. Hoskins, T. Anderson, M. Sharp, S. Meagher, T. McGillivray, and W. N. McDicken, "Ultrasound B-mode 360-deg tomography in mice," *IEEE Ultrason. Symp. Proc.* 752–755 (2004).
26. F. C. Breedveld, "New perspectives on treating rheumatoid arthritis [editorial comment]," *N. Engl. J. Med.* **333**, 183–184 (1995).
27. P. Emery, "Evidence supporting the benefit of early intervention in rheumatoid arthritis," *J. Rheumatol.* **29**, 3–8 (2002).
28. Y. Xu, N. Iftimia, and H. Jiang, "Imaging of *in vitro* and *in vivo* bones and joints with continuous-wave diffusion optical tomography," *Opt. Express* **8**, 447–451 (2001).
29. Y. Xu, N. Iftimia, H. Jiang, L. L. Key, and M. B. Bolster, "Three-dimensional diffuse optical tomography of bones and joints," *J. Biomed. Opt.* **7**, 88–92 (2002).
30. J. Beuthan, U. Netz, O. Minet, A. D. Klose, A. H. Hielscher, A. Scheel, J. Henniger, and G. Muller, "Light scattering study of rheumatoid arthritis," *Quantum Electron.* **32**, 945–952 (2002).